Acta Crystallographica Section D
Biological Crystallography
ISSN 1399-0047

Structural elucidation of the hormonal inhibition mechanism of the bile acid cholate on human carbonic anhydrase II

Christopher D. Boone,[a] Chingkuang Tu[b] and Robert McKenna[a]*

[a]Department of Biochemistry and Molecular Biology, University of Florida, PO Box 100267, Gainesville, FL 32610, USA, and [b]Department of Pharmacology and Therapeutics, University of Florida, PO Box 100245, Gainesville, FL 32610, USA

Correspondence e-mail: rmckenna@ufl.edu

Received 5 February 2014
Accepted 3 April 2014

PDB reference: human carbonic anhydrase II–cholate complex, 4n16

The carbonic anhydrases (CAs) are a family of mostly zinc metalloenzymes that catalyze the reversible hydration/dehydration of CO_2 into bicarbonate and a proton. Human isoform CA II (HCA II) is abundant in the surface epithelial cells of the gastric mucosa, where it serves an important role in cytoprotection through bicarbonate secretion. Physiological inhibition of HCA II *via* the bile acids contributes to mucosal injury in ulcerogenic conditions. This study details the weak biophysical interactions associated with the binding of a primary bile acid, cholate, to HCA II. The X-ray crystallographic structure determined to 1.54 Å resolution revealed that cholate does not make any direct hydrogen-bond interactions with HCA II, but instead reconfigures the well ordered water network within the active site to promote indirect binding to the enzyme. Structural knowledge of the binding interactions of this nonsulfur-containing inhibitor with HCA II could provide the template design for high-affinity, isoform-specific therapeutic agents for a variety of diseases/pathological states, including cancer, glaucoma, epilepsy and osteoporosis.

1. Introduction

The carbonic anhydrases (CAs; EC 4.2.1.1) are mostly zinc-containing metalloenzymes that are important in acid–base homeostasis as they catalyze the reversible hydration of CO_2 into bicarbonate and a proton (Boone *et al.*, 2014). Several isoforms of human CAs (HCAs) along the gastrointestinal tract, including HCA II, are inhibited by the bile acids (BAs; Milov *et al.*, 1992), the primary products of cholesterol catabolism (Staels & Fonseca, 2009). BAs have been shown to damage the gastric mucosa in animals, and duodenogastric reflux is regarded as one pathogenic factor in gastritis, gastric ulcer and alkaline reflux gastritis in the postgastrectomy stomach in humans (Salomoni *et al.*, 1989). The mucosal damaging activity of cholic acid, taurocholic acid and glycochenodeoxycholic acid has been directly associated with gastric mucosal CA inhibition in rats and humans (Kivilaakso, 1982). The BAs have been shown to be transported into the cytosol of biliary epithelial cells (Benedetti *et al.*, 1997). The immediate products of the BA synthetic pathways (cholic acid and chenodeoxycholic acid) are referred to as the primary BAs, whereas dehydroxylation from C7 of the sterane core of either primary BA *via* the action of the gut bacterial flora constitutes the secondary BAs deoxycholic and lithocholic acid (Fig. 1). The hydrophilicity of the BAs can be further enhanced before secretion into the bile canalicular lumen of the gall bladder for storage *via* conjugation with taurine or glycine (Staels & Fonseca, 2009). The strongest binding

Table 1
Macromolecule-production information.

Source organism	Human
DNA source	Human carbonic anhydrase II
Forward primer	*Eco*RI, *Bgl*II, *Hin*dIII
Reverse primer	*Xho*I
Cloning vector	*E. coli* XL1-Blue
Expression vector	pET-23b
Expression host	*E. coli* BL21(DE3)
Complete amino-acid sequence of the construct produced	MSHHWGYGKHNGPEHWHKDFPIAKGERQSPVDIDTHT-AKYDPSLKPLSVSYDQATSLRILNNGHAFNVEFD-DSQDKAVLKGGPLDGTYRLIQFHFHWGSLDGQGS-EHTVDKKKYAAELHLVHWNTKYGDFGKAVQQPDG-LAVLGIFLKVGSAKPGLQKVVDVLDSIKTKGKSA-DFTNFDPRGLLPESLDYWTYPGSLTTPPLLECVT-WIVLKEPISVSSEQVLKFRKLNFNGEGEPEELMV-DNWRPAQPLKNRQIKASFK

affinity among the BAs for HCA II include cholic and deoxycholic acid, with I_{50} values of ∼0.1 and 0.4 m*M*, respectively, as measured using stopped-flow spectrophotometry studies (Salomoni *et al.*, 1989).

Structural knowledge of the binding interactions of the BAs to HCA II would promote further insights into gastric ulcer development and aid in the design of a therapeutic agent that displays isoform inhibition specificity among the HCAs. The inhibition of HCA II has been utilized for the treatment of various diseases in the past, including glaucoma, epilepsy and altitude sickness (Supuran, 2008). Current clinically used inhibitors of HCA II include acetazolamide and brinzolamide, which incorporate a sulfonamide functional head group, have detrimental side effects including augmented diaeresis, fatigue, paresthesias and anorexia owing to the nonspecific inhibition of CA isoforms in other tissues than those targeted (Aggarwal *et al.*, 2013). Additionally, an estimated 3% of the total population has an adverse drug reaction to sulfonamide-containing compounds, with higher rates of sulfa allergies seen in individuals with low metabolic process rates and in immunocompromised patients (Choquet-Kastylevsky *et al.*, 2002). Thus, BA inhibition of HCA II is an attractive therapeutic agent as they are nonsulfur-containing compounds that are easily transported across the cellular membrane and

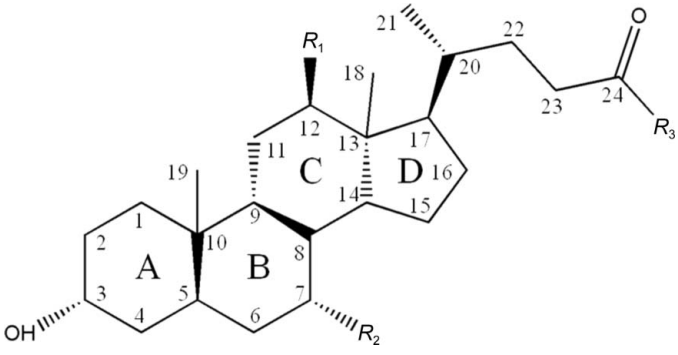

Figure 1
Schematic of the BA sterane core and substituents. C atoms and ring systems are labeled according to IUPAC numbering. The hydroxylation/dehydroxylation of R_1 and R_2, along with conjugation of a hydroxyl, taurine or glycine group at R_3, constitutes the various BAs.

Table 2
Crystallization.

Method	Hanging-drop vapor diffusion
Plate type	VDXm 24-well
Temperature (K)	298
Protein concentration (mg ml^{-1})	10
Buffer composition of protein solution	50 m*M* Tris–HCl pH 7.8
Composition of reservoir solution	1.6 *M* sodium citrate, 50 m*M* Tris–HCl pH 7.8
Volume and ratio of drop	5 µl; 1:1 protein:reservoir
Volume of reservoir (µl)	500

are extremely soluble in water compared with conventional drugs such as acetazolamide and methazolamide.

2. Methods

2.1. Enzyme expression and purification

HCA II cDNA containing the enzyme-coding region (Forsman *et al.*, 1988) was transformed into *Escherichia coli* XL1-Blue Supercompetent cells, which were then confirmed by DNA sequencing of the entire coding region (Table 1). The HCA II cDNA was then transformed into *E. coli* BL21(DE3) cells in 1 l 2× Luria broth medium containing ∼0.1 mg ml^{-1} ampicillin and grown at 37°C to a turbidity of ∼0.6 at 600 nm. Protein production was induced by the addition of ∼0.1 mg ml^{-1} isopropyl β-D-1-thiogalactopyranoside (IPTG) and ∼1 m*M* zinc sulfate (final concentrations). The cells were incubated for an additional 3 h and harvested by centrifugation.

A suspension of cells in 200 m*M* sodium sulfate, 100 m*M* Tris–HCl pH 9.0 was lysed by the addition of hen egg-white lysozyme and DNaseI with subsequent removal of cellular debris by centrifugation. The enzyme was purified on an affinity column containing an agarose resin coupled with *p*-(aminomethyl)benzenesulfonamide, a tight-binding inhibitor of HCA II (Khalifah *et al.*, 1977). The bound HCA II was eluted with 400 m*M* sodium azide, 100 m*M* Tris–HCl pH 7.0 followed by extensive dialysis in 50 m*M* Tris–HCl pH 7.8 to remove the azide. The purified enzyme was concentrated to ∼10 mg ml^{-1} for crystallization studies *via* centrifugal ultrafiltration using a 10 kDa molecular-weight cutoff filter (Amicon). The purity of the sample was visualized *via* SDS–PAGE and was determined to be >95% (data not shown).

2.2. Crystallization and diffraction data collection

Crystals of HCA II formed after one week in a 1:1 ratio of protein:reservoir solution in 5 µl drops using the hanging-drop vapor-diffusion method against 500 µl reservoir solution consisting of 1.6 *M* sodium citrate, 50 m*M* Tris–HCl pH 7.8. 1 µl 100 m*M* cholate was dissolved in 50 m*M* Tris–HCl pH 7.8 and was added to the crystal drop to a final concentration of ∼17 m*M* for 4 h prior to data collection (Table 2). The crystal was further washed for 10 s in cryoprotectant containing an equivalent concentration of cholate dissolved in the mother liquor and 20%(*w*/*v*) glycerol prior to data collection.

Table 3
Data collection and processing.

Values in parentheses are for the outer shell.

Diffraction source	Rotating copper anode
Wavelength (Å)	1.5418
Temperature (K)	100
Detector	Rigaku R-AXIS IV^{++} image plate
Crystal-to-detector distance (mm)	80
Rotation range per image (°)	1
Total rotation range (°)	180
Exposure time per image (s)	300
Space group	$P2_1$
a, b, c (Å)	42.4, 41.6, 71.9
α, β, γ (°)	90.0, 104.5, 90.0
Mosaicity (°)	0.86
Resolution range (Å)	20–1.54 (1.60–1.54)
Total No. of reflections	124916
No. of unique reflections	33813
Completeness (%)	93.6 (89.8)
Multiplicity	3.7 (3.7)
$\langle I/\sigma(I)\rangle$	26.9 (2.9)
$R_{\rm meas}$†	0.052 (0.516)
Overall B factor from Wilson plot (Å^2)	21.7

† $R_{\rm meas}$ is defined as $\sum_{hkl}\{N(hkl)/[N(hkl)-1]\}^{1/2}\sum_i |I_i(hkl)-\langle I(hkl)\rangle|/\sum_{hkl}\sum_i I_i(hkl)$, where $I_i(hkl)$ is the intensity of an individual reflection, $\langle I(hkl)\rangle$ is the average intensity for this reflection and $N(hkl)$ is the multiplicity (Diederichs & Karplus, 1997).

Table 4
Structure solution and refinement.

Values in parentheses are for the outer shell.

Resolution range (Å)	20.0–1.54 (1.59–1.54)
Completeness (%)	93.5 (89.0)
σ Cutoff	1.35
No. of reflections, working set	32134
No. of reflections, test set	1678
Final $R_{\rm cryst}$† (%)	14.7
Final $R_{\rm free}$‡ (%)	17.4
No. of non-H atoms	
Protein	2287
Ion	1
Ligand	26
Water	265
Total	2579
R.m.s. deviations	
Bonds (Å)	0.009
Angles (°)	1.308
Average B factors (Å^2)	
Protein	9.0
Ion	3.8
Ligand	13.0
Water	24.3
Ramachandran plot	
Most favored (%)	97.3
Allowed (%)	2.7

† $R_{\rm cryst}=\sum_{hkl}\big||F_{\rm obs}|-|F_{\rm calc}|\big|/\sum_{hkl}|F_{\rm obs}|\times 100$. ‡ $R_{\rm free}$ is calculated in the same way as $R_{\rm cryst}$ except using data omitted from refinement (5% of reflections).

Diffraction data were collected at 100 K on an in-house Rigaku R-AXIS IV^{++} image-plate detector using an RU-H3R rotating Cu anode ($K\alpha$ = 1.5418 Å) operating at 50 kV and 22 mA with a crystal-to-detector distance of 80 mm. The X-rays were focused using Osmic optics followed by a helium-purged beam path. Diffraction data were collected with 1° oscillations and an exposure time of 300 s per image. *HKL*-2000 (Otwinowski & Minor, 1997) was used to integrate, merge and scale the data in the monoclinic space group $P2_1$ to a final resolution of 1.54 Å. A summary of the data statistics is provided in Table 3.

2.3. Structure refinement

Initial phases for the HCA II–cholate complex were calculated *via* molecular replacement using *Phaser* (McCoy *et al.*, 2007) with the coordinates of the high-resolution HCA II structure (PDB entry 3ks3; Avvaru *et al.*, 2010). Electron density in the initial $mF_{\rm o}-DF_{\rm c}$ maps revealed positive density at >5σ suggesting cholate binding in the active site of HCA II. *Phenix.refine* (Afonine *et al.*, 2012) was used in cycles of restrained refinement of the molecular model alternating with manual building using *Coot* (Emsley & Cowtan, 2004). Solvent molecules that refined to B factors of more than 50 Å^2 were excluded from the final model. The $R_{\rm cryst}$ and $R_{\rm free}$ values for the final model were 14.7 and 17.4%, respectively. *MolProbity* (Chen *et al.*, 2010) was used to assess the quality of the final model. 97.3% of the residues were in the most favored conformations and 2.7% were in generously allowed regions. The final model statistics are given in Table 4. All crystallographic figures were generated in *PyMOL* (http://www.pymol.org). Experimental data and structural coordinates have been deposited in the Protein Data Bank under accession code 4n16.

2.4. Inhibition studies

An ^{18}O-exchange assay was carried out to study the kinetics of the catalyzed HCO_3^-–CO_2 dehydration–hydration reaction and its bile acid inhibition at 283 K. This method relies on the depletion of ^{18}O from CO_2 as measured by membrane-inlet mass spectrometry. CO_2 passing across the membrane of the inlet enters a mass spectrometer (Extrel EXM-200), providing a continuous measure of the isotopic content of CO_2 in solution. In the first stage of catalysis, the dehydration of labelled bicarbonate has a probability of transiently labelling the active site with ^{18}O. In a subsequent step, protonation of the zinc-bound ^{18}O-labeled hydroxide results in the release of $H_2^{18}O$ into the solvent.

I_{50} values were obtained for cholate and deoxycholate in 100 m*M* HEPES pH 8.0. Dissolved bile acids (100 m*M*) in 100 m*M* Tris pH 7.8 were titrated against HCA II (at a nanomolar concentration) in 10 µl aliquots until isotopic quenching of ^{18}O had occurred.

3. Results and discussion

The X-ray crystallographic structure of cholate bound to HCA II was refined to a resolution of 1.54 Å, with the final model (Fig. 2*a*) having $R_{\rm cryst}$ and $R_{\rm free}$ values of 14.7 and 17.4%, respectively. Summaries of the collected diffraction data and final refinement statistics are given in Tables 3 and 4, respectively. Initial $mF_{\rm o}-DF_{\rm c}$ difference maps obtained *via* mole-

cular replacement using the high-resolution model of HCA II (PDB entry 3ks3) revealed strong (>5σ) positive peak density for the cholate ligand bound in the active site (Fig. 2*b*). The observed values of I_{50} were based on measurement of the catalytic activity of HCA II by ^{18}O mass spectrometry and revealed weak binding affinity for cholate (~0.2 m*M*; Fig. 3*a*) and deoxycholate (~0.4 m*M*; Fig. 3*b*). These values agree well with the inhibition data obtained in previous stopped-flow experiments (~0.1 and 0.4 m*M*, respectively; Kivilaakso, 1982).

The natural epimerization of the hydroxyl and methyl moieties on the sterane core (Fig. 1) presents an optimal configuration for cholate to interact with the opposing hydrophilic and hydrophobic faces found within the active site of HCA II (Fig. 2*c*). The hydrophobic residues Ile91, Val121, Phe131, Leu141 and Leu198 are observed to have a significant buried surface area (>50%) upon cholate binding. Of these hydrophobic interfaces, Phe131 and Leu198 are observed to undergo the largest conformational shift (~0.7–0.8 Å) upon ligation. Interestingly, Phe131 is highly variable among the human CA isozymes [*i.e.* Val in HCA IX (Alterio *et al.*, 2009) and Ala in HCA XII (Whittington *et al.*, 2001), two isoforms overexpressed on the surface of tumor cells]. Utilization of the slight hydrophobicity differences in the active site of these CAs overexpressed in an wide array of cancer lines could provide a site for isoform specificity.

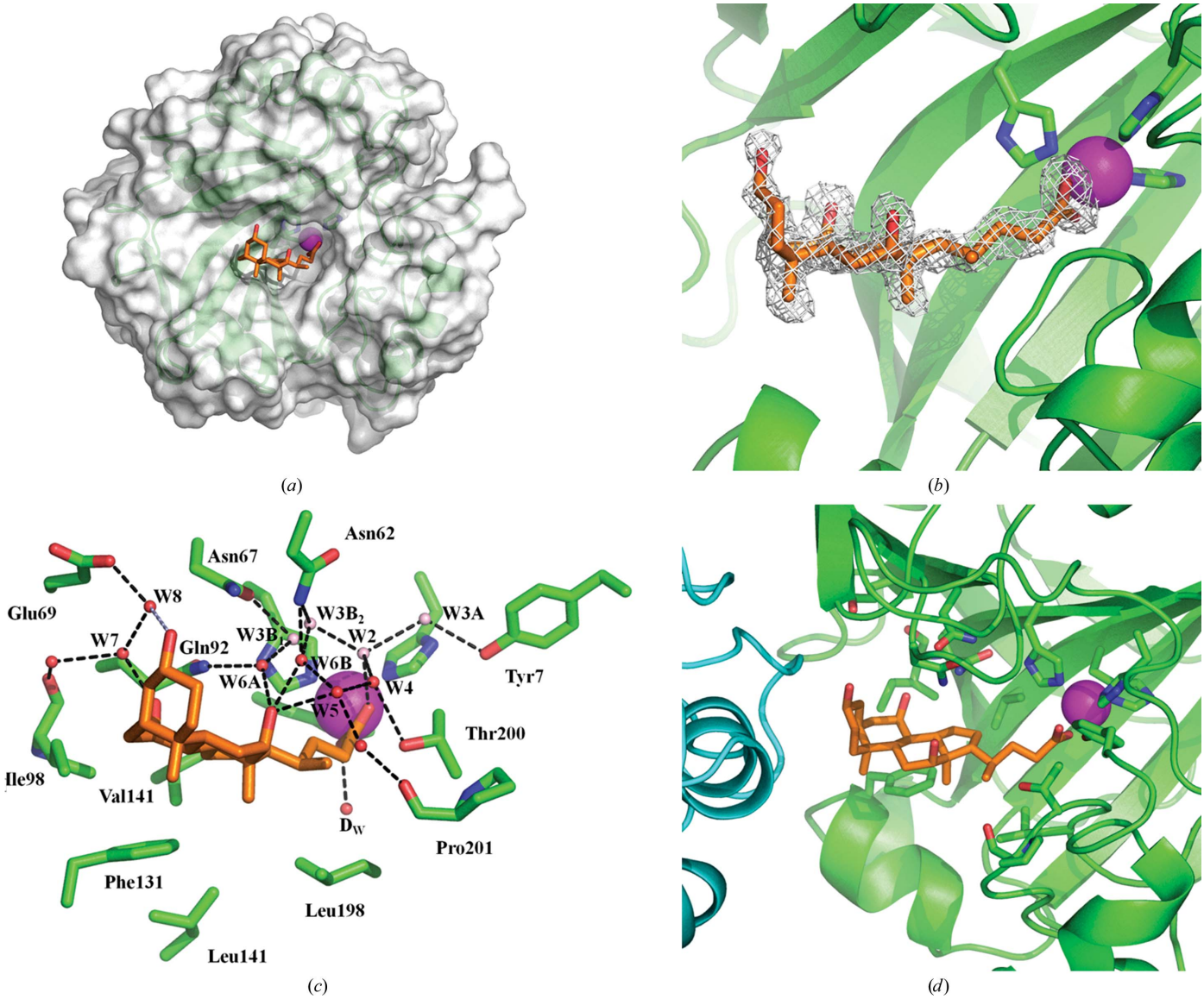

Figure 2
X-ray crystallographic structure of cholate binding to HCA II. (*a*) Surface view of cholate (orange sticks) binding into the active site of HCA II (transparent gray surface). The C$^{\alpha}$ backbone is shown as a cartoon view in green. The Zn^{2+} metal ion is shown as a magenta sphere. (*b*) Initial $mF_o - DF_c$ map (gray mesh) contoured at 2.0σ of cholate bound in the active site of HCA II. (*c*) Hydrogen-bond interactions (black dashed lines) between cholate and the surrounding water molecules (red spheres). Interacting residues and water molecules are as labeled. The water molecules important in the proton-transfer mechanism (W2, W3A, $W3B_1$ and $W3B_2$) are shown as light pink spheres. (*d*) Crystal packing depicting the crystallographic symmetry molecule $-x + 1, y - 1/2, -z + 2$ (cyan C$^{\alpha}$ cartoon).

The hydroxyl groups of cholate do not make any potential strong hydrogen-bond interactions with the hydrophilic face of the HCA II active site. Instead, cholate is observed to utilize a series of water molecules that provide a weak connection between the enzyme and ligand (Fig. 2*c*). Cholate is seen to bind to the zinc ion in a bivalent interaction centralized between the two O atoms of the carboxyl group which displaces the zinc-bound solvent molecule and water 1 (W1) of the proton-transfer water network (Boone *et al.*, 2014). The carboxyl O atoms are also at potential hydrogen-bonding distance from two well ordered water molecules observed in the unbound active site termed the deep water (D_W), which acts as a place holder for CO_2 binding, and W2, which is involved in the transfer of a proton from the zinc-bound solvent to His64 (Boone *et al.*, 2014). The D_W molecule has been displaced 0.9 Å further into the hydrophobic pocket of the CO_2-binding site towards Trp209 upon binding cholate, whereas the zinc-bound solvent molecule W2 is in an comparable position to that in the unbound structure.

The branching water molecules involved in hydrogen bonding to Tyr7 and Asn62/67 (W3A and W3B, respectively, in unbound HCA II) are also observed in the cholate-bound structure. W2 and W3A are observed in comparable positions to those in the unbound structure, whereas W3B accompanies two distinguishable binding sites ∼0.5 Å apart, termed $W3B_1$ and $W3B_2$, with ∼60 and 40% occupancy, respectively. $W3B_1$ is within hydrogen-bonding distance of $N^{\delta2}$ of Asn62 (3.0 Å), which has shifted ∼0.7 Å compared with the unbound structure. The lower occupancy $W3B_2$ molecule is within 2.6 Å of $N^{\delta2}$ of Asn67, which has been flipped from its position in the unbound structure, in which W3B interacts with $O^{\delta1}$ of Asn67. The relatively high *B* factor for $O^{\delta1}$ of Asn67 (45 *versus* ∼20 Å^2 on average) and the weak electron density in the $2mF_o - DF_c$ map (maximum peak at ∼0.7 e Å^{-3}) suggests dynamic hydrogen-bond interactions between this carbonyl O atom amd $N^{\delta2}$ of Asn62, $N^{\varepsilon2}$ of Gln92 and a low-occupancy (<10%) diffuse water. Movement of $N^{\varepsilon2}$ of Gln92 by ∼1.6 Å compared with the unbound structure places it in position for a potential hydrogen bond to W6B (2.9 Å) and a weak direct interaction with the C7 hydroxyl group of cholate (3.5 Å). The C12 hydroxyl is observed to make potential hydrogen-bond interactions with W5 (2.8 Å), W6A and W6B (∼2.8 Å), which are present 1.7 Å from one another with ∼50% occupancy each (Fig. 2*c*). W6A makes a potential hydrogen bond to $N^{\delta2}$ in Asn62 (2.6 Å), whereas W6B interacts with N^{ε} of Gln92 (above). The movements of $W3A_1$ to $W3B_2$ with W6A to W6B may be correlated as they are ∼2.4 Å from one another with comparable occupancies. The thermal fluncuations seen in $O^{\delta1}$ of Asn67 may be the driving force behind these alternate states of W3B and W6. W5 interacts with a neighboring water molecule (2.6 Å) which is within hydrogen-bonding distance of the carbonyl backbone of Pro201 (2.7 Å). W5 and W2 also bond to W4, which is within hydrogen-bonding distance of Thr200. W4 is commonly seen in other HCA II–inhibitor structures when His64 is locked into the 'outward' configuration (Fisher, Aggarwal *et al.*, 2012). The C7 hydroxyl is within hydrogen-bonding distance of W7 (2.4 Å), which binds to an adjacent water molecule that interacts with the backbone carbonyl O atom of Ile91.

The C3 hydroxyl group is seen to be within hydrogen-bonding distance of W8 (2.6 Å; Fig. 2*c*, white dashed line), which makes a hydrogen bond to Glu69 and W7. Closer inspection of the crystallographic structure revealed an ∼90° tilt of ring A in the sterane core that is most likely owing to close contact of residues 235–238 on a symmetry-related molecule ($-x + 1$, $y - 1/2$, $-z + 2$) near the opening of the active site of the molecule in the asymmetric unit (Fig. 2*d*) and may not be biologically significant.

Crystallization of the conjugated BAs (*e.g.* glycocholate) with HCA II may be limited owing to the steric interference of symmetry-related molecules within the monoclinic unit cell (Fig. 2*d*) and may require studies in a different space group, such as $P2_12_12_1$, that increases the accessibility of the active site (Fisher, Boone *et al.*, 2012). Attempts to observe deoxycholate in the active site of HCA II were limited owing to lowered solubility and higher critical micellular concentrations compared with cholate, but a weaker binding affinity can be extrapolated as dehydroxylation from C7 would correspond to

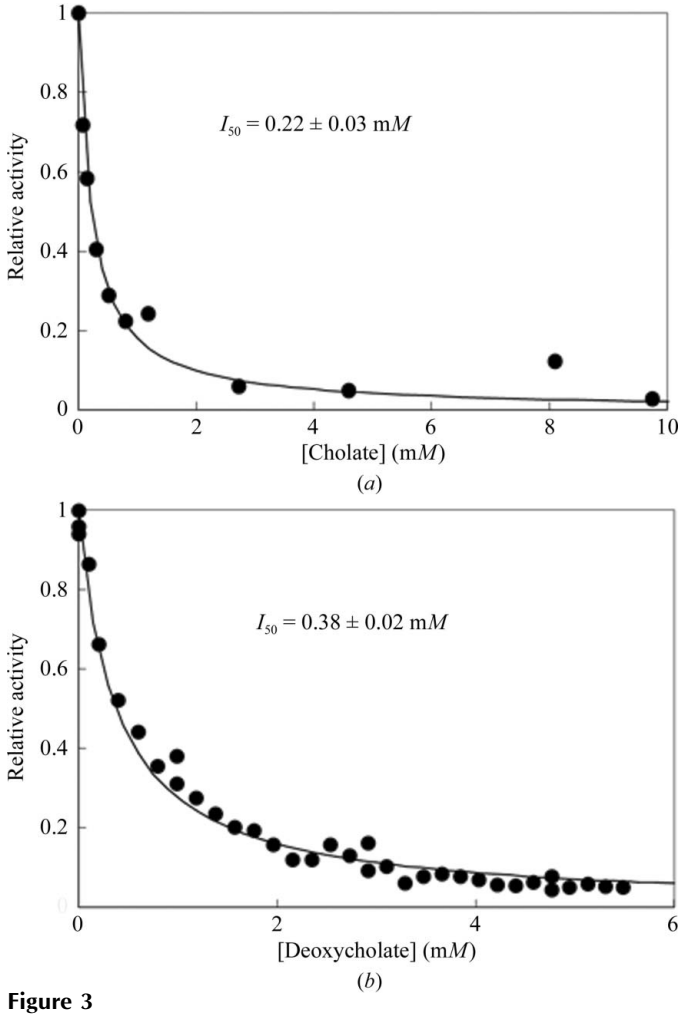

Figure 3
Determination of I_{50} from catalytic activity measured by mass spectrometry using ^{18}O-labeled substrates for (*a*) cholate and (*b*) deoxycholate. I_{50} values are inset.

broken hydrogen bonds between W5 and W6A/B (Fig. 2*c*). Implementation of substituents on the sterane core that establish direct hydrogen bonds among the active-site residues, such as Asn67 in HCA II (Gln67 in HCA IX), could provide a template for a tight-binding, isoform-specific therapeutic cancer agent.

This research has partially been funded by the NIH (GM25154). The authors would like to thank the Center of Structural Biology for support of the X-ray facility at UF. We thank David Silverman for helpful comments.

References

Afonine, P. V., Grosse-Kunstleve, R. W., Echols, N., Headd, J. J., Moriarty, N. W., Mustyakimov, M., Terwilliger, T. C., Urzhumtsev, A., Zwart, P. H. & Adams, P. D. (2012). *Acta Cryst.* D**68**, 352–367.

Aggarwal, M., Kondeti, B. & McKenna, R. (2013). *Bioorg. Med. Chem.* **21**, 1526–1533.

Alterio, V., Hilvo, M., Di Fiore, A., Supuran, C. T., Pan, P., Parkkila, S., Scaloni, A., Pastorek, J., Pastorekova, S., Pedone, C., Scozzafava, A., Monti, S. M. & De Simone, G. (2009). *Proc. Natl Acad. Sci. USA*, **106**, 16233–16238.

Avvaru, B. S., Kim, C. U., Sippel, K. H., Gruner, S. M., Agbandje-McKenna, M., Silverman, D. N. & McKenna, R. (2010). *Biochemistry*, **49**, 249–251.

Benedetti, A., Di Sario, A., Marucci, L., Svegliati-Baroni, G., Schteingart, C. D., Ton-Nu, H. T. & Hofmann, A. F. (1997). *Am. J. Physiol.* **272**, G1416–G1424.

Boone, C. D., Pinard, M., McKenna, R. & Silverman, D. (2014). *Carbonic Anhydrase: Mechanism, Regulation, Links to Disease, and Industrial Applications*, edited by S. C. Frost & R. McKenna, pp. 31–52. New York: Springer.

Chen, V. B., Arendall, W. B., Headd, J. J., Keedy, D. A., Immormino, R. M., Kapral, G. J., Murray, L. W., Richardson, J. S. & Richardson, D. C. (2010). *Acta Cryst.* D**66**, 12–21.

Choquet-Kastylevsky, G., Vial, T. & Descotes, J. (2002). *Curr. Allergy Asthma Rep.* **2**, 16–25.

Diederichs, K. & Karplus, P. A. (1997). *Nature Struct. Biol.* **4**, 269–275.

Emsley, P. & Cowtan, K. (2004). *Acta Cryst.* D**60**, 2126–2132.

Fisher, S. Z., Aggarwal, M., Kovalevsky, A. Y., Silverman, D. N. & McKenna, R. (2012). *J. Am. Chem. Soc.* **134**, 14726–14729.

Fisher, Z., Boone, C. D., Biswas, S. M., Venkatakrishnan, B., Aggarwal, M., Tu, C., Agbandje-McKenna, M., Silverman, D. & McKenna, R. (2012). *Protein Eng. Des. Sel.* **25**, 347–355.

Forsman, C., Behravan, G., Osterman, A. & Jonsson, B. H. (1988). *Acta Chem. Scand.* **B42**, 314–318.

Khalifah, R. G., Strader, D. J., Bryant, S. H. & Gibson, S. M. (1977). *Biochemistry*, **16**, 2241–2247.

Kivilaakso, E. (1982). *Am. J. Surg.* **144**, 554–557.

McCoy, A. J., Grosse-Kunstleve, R. W., Adams, P. D., Winn, M. D., Storoni, L. C. & Read, R. J. (2007). *J. Appl. Cryst.* **40**, 658–674.

Milov, D. E., Jou, W. S., Shireman, R. B. & Chun, P. W. (1992). *Hepatology*, **15**, 288–296.

Otwinowski, Z. & Minor, W. (1997). *Methods Enzymol.* **276**, 307–326.

Salomoni, M., Zuccato, E., Granelli, P., Montorsi, W., Doldi, S. B., Germiniani, R. & Mussini, E. (1989). *Scand. J. Gastroenterol.* **24**, 28–32.

Staels, B. & Fonseca, V. A. (2009). *Diabetes Care*, **32**, S237–S245.

Supuran, C. T. (2008). *Nature Rev. Drug Discov.* **7**, 168–181.

Whittington, D. A., Waheed, A., Ulmasov, B., Shah, G. N., Grubb, J. H., Sly, W. S. & Christianson, D. W. (2001). *Proc. Natl Acad. Sci. USA*, **98**, 9545–9550.